SLAC–PUB–6724
January 1996

A COAXIAL RING–SIDEARM POWER EXTRACTION DESIGN*

Shahar Ben-Menahem° and David Yu

DULY Research Inc.
1912 MacArthur Street
Rancho Palos Verdes, CA 90275
and
Stanford Linear Accelerator Center
Stanford University, Stanford, California 94309

Presented at the Pulsed RF Sources for Linear Colliders Conference
Montauk, New York, October 2–7, 1994

*Work supported in part by Department of Energy SBIR Grant DE–FG03–93ER81573 (DULY) and by Department of Energy contract DE–AC03–76SF00515 (SLAC).
°Visitor to the Accelerator Theory and Special Projects Group at the Stanford Linear Accelerator Center, Stanford University, Stanford, California 94309.

ABSTRACT

We report on a successful klystron power extraction design, in which a TEM coaxial mode is transmitted into the TE10 mode of a WR90 rectangular waveguide at 11.42 GHz, with very little TEM reflection and almost vanishing asymmetric (TEM → TE11, or monopole to dipole) reflectance. Our coupler consists of a ring (disk) around the coaxial waveguide, and a coax-WR90 sidearm junction (see Fig. 1). The methods used in the design are numerical simulation, performed on the MAFIA3 T3 time-domain module and on the High Frequency Structure Simulator (HFSS), and analytical treatment to guide the numerical runs. The demerit parameters (dipole reflectance and TEM reflection) can be reduced as much as desired (to zero in principle), the only limitation being computer run time and memory. The results reported are accurate to a few percent.

1. Background

The coaxial ring-sidearm power extraction modeling described in this paper is part of a preliminary cold-test design for a coaxial power-output coupler. The Cluster Klystron Power Combiner, under development by DULY Research in collaboration with researchers from SLAC and BNL, utilizes three subklystrons, with the rf energy from each fed into the Combiner junction via such a coaxial coupler.

2. Spatial Constraints

The geometry used for a realistic coax-ring-sidearm rf output coupler for the Cluster Klystron Power Combiner is severely constrained. Coax dimensions must be such as to:

(a) couple out the TEM mode efficiently from the subklystron Traveling Wave Structure;

(b) not excite too many coaxial modes;

(c) disallow propagation of modes interior to inner coax tube; and

(d) allow, nevertheless, enough transverse extent inside the inner tube to conduct the spent subklystron beam to the beam dump.

Additional constraints involve ensuring that the three subklystrons are able to physically fit together. The design described here satisfies conditions (a) through (d), but not the fitting constraints. Work is in progress to adapt our design methodology to realistic dimensions—including different coaxial radii—and also to properly take into account the dynamical effects of the beam.

3. Coax Dimensions and Coordinate Definitions

For the test design, we used the following outer and inner coax radii:

$$r_{\rm out} = 0.433 \quad \text{inches}\,, \qquad r_{\rm in} = 0.193 \quad \text{inches} \quad . \tag{1}$$

For these radii, and at $f = 11.42$ GHz, the only propagating modes are:

$$\begin{aligned} TEM \;\; [\beta = 239.3\ \mathrm{m}^{-1}] \quad , \\ TE11 \;\; [\beta = 202.4\ \mathrm{m}^{-1}] \quad , \end{aligned} \tag{2}$$

with an evanescent quadrupole mode having a low enough alpha value ($\alpha \approx 73\ \mathrm{m}^{-1}$) to affect the design. We simulate only a half-structure, so we have only a single TE11 mode to deal with.

For comparison, a more realistic set of coax radii would be

$$r_{\rm out} = 12\ \text{mm}\,, \qquad r_{\rm in} = 7\ \text{mm} \quad , \tag{3}$$

for which TEM has the same beta value; $\beta\,(TE11) = 214.6\ \mathrm{m}^{-1}$; and the quadrupole mode is now propagating at about

$$\beta\,(\text{quad}) \;\approx\; 113\ \mathrm{m}^{-1} \quad . \tag{4}$$

The coordinate axes are defined as follows (see Figs. 1–3). The coax axis, pointing into the junction, is Z. The Y axis points along the WR90 waveguide axis, away from the junction. Only the $x > 0$ half of the geometry is modeled. The origin is chosen to lie on the coax axis and in the middle of the WR90 height, which is along the Z-axis. The YZ plane ($x = 0$) is treated as a magnetic symmetry wall.

4. Design Strategy

We design the coax-WR90 sidearm following the Slater geometry, with both the WR90 and coax continuing past their junction to form stubs. We are able to choose the coaxial stub (referred to below as z-stub, since it is in the Z direction) such that the TEM $\rightarrow$ TE11 asymmetric reflectance amplitude is extremely small (0.005 according to HFSS, and 0.002 according to MAFIA). In principle, it could be made to vanish. We then choose dimensions and position for the coaxial ring, upstream of the junction, so as to match the TEM sidearm reflectance. Thus the TEM reflectance of the overall structure amplitude comes out about 0.15 in MAFIA and 0.18 in HFSS. Again, in principle, this demerit figure can be reduced to zero.

5. Theory, Simulation and Optimization

5.1 Theory versus simulation

The geometry of the complete output structure (sidearm, coax, and ring) is shown in Figs. 1 and 2. Figure 1 is generated by HFSS. Figure 2 includes the optimized dimensions we obtained. The sidearm contains a short at $y = y_{\min} = -r_{\text{out}} - y_{\text{stub}}$, with r_{out} the outer coax radius and y_{stub} the WR90 stub length. For theoretical analysis, we found it useful to begin by opening this short. Likewise, we open the short at the end of the coax stub on the plane $z = z_{\max} = 0.2$ inches $+ z_{\text{stub}}$, with z_{stub} the coaxial-stub length and 0.2 inches the WR90 half-height.

Upon opening these two shorts into ports, we end up with a junction structure that has four ports—two coaxial and two rectangular. By properly adjusting the

positions of the four port planes, we obtain a highly symmetric HALF-JUNCTION STRUCTURE; it has the following two new symmetries:

$$\begin{aligned} y &\rightarrow -y \quad , \\ z &\rightarrow -z \quad . \end{aligned} \tag{5}$$

We then cut this half-structure in half, by keeping only the $y > 0$ portion thus yielding the QUARTER-JUNCTION STRUCTURE depicted in Fig. 3 (which still has the residual symmetry $z \rightarrow -z$).

Our analysis next consists of the following stages:

(A) High precision, separate simulations of the quarter-junction structure and of the ring, which is also reduced to a quarter structure to facilitate simulation. Obviously, each such quarter-structure needs to be run twice—once for TEM boundary conditions (b.c.) which involves two magnetic symmetry walls, and once for TE11 b.c. which involves one magnetic wall and one electric wall.

(B) Restoring the two shorts at $y_{\min}$ and $z_{\max}$; the resulting sidearm S-matrix is determined analytically from the numerical results of stage (A). The length z_{stub} is analytically adjusted to yield zero theoretical TEM $\rightarrow$ TE11 reflectance.

(C) The sidearm S-matrix of stage (B) is compared with a simulation of the sidearm for various stub lengths y_{stub} and z_{stub}.

(D) Values of $(y_{\text{stub}}, z_{\text{stub}})$, and ring geometry, are chosen so that TEM $\rightarrow$ TEM reflectances of ring and sidearm match, and such that TEM $\rightarrow$ TE11 reflectance maintains the value 0.

(E) Using both theory and simulations, the distance L between ring and WR90 is optimized to yield zero (in practice, small) TEM reflectance for the combined output structure.

In practice, we find that the theoretical determination of the optimal coaxial stub length, $z_{\rm stub}$, in stage (B) above agrees quite well with the simulations. Furthermore, the optimal $z_{\rm stub}$ appears to be independent of $y_{\rm stub}$, as predicted by theory. We are thus able, using the quarter-junction S-matrix of stage (A), to immediately find a whole class of sidearm designs with vanishing TEM $\rightarrow$ TE11 reflectances—greatly simplifying the optimization task. In stage (C), however, we find a significant discrepancy between theory and simulation. We attribute this to evanescent modes excited in the sidearm structure, notably the quadrupole mode mentioned above. Despite this discrepancy, the theoretical analysis of stage (B) is a useful guide to choosing possible values of $y_{\rm stub}$. In stage (E) (optimization of the ring-WR90 distance, L), theory is again found to be rather accurate.

5.2 Analytical details and numerical results

For the quarter-junction structure (see Fig. 3), we use the following notation* for the S-matrix elements:

$$S^q_{\bar{1}\bar{1}}\,,\quad S^q_{\bar{2}\bar{2}}\,,\quad S^q_{33}\,,\quad S^q_{\bar{1}3}\,,\quad S^q_{\bar{2}3}\,,\quad \widetilde{S}^q_{33}\quad , \tag{6}$$

where the superscript 'q' denotes 'quarter structure' and 1, 2, 3 denote the TEM, coaxial TE11 and rectangular TE10 modes, respectively. We also denote by $\bar{1},\bar{2}$ the TEM and TE11 modes at the $z_{\rm max}$ port, to distinguish from 1, 2 (which denote the same modes at the $z_{\rm min}$ coax port). By the $z\rightarrow -z$ symmetry, and the fact that the TE10 WR90-mode has $\vec{E}$ along the Z direction, we find:

$$\begin{aligned} S^q_{\bar{1}\bar{1}} &= -S^q_{\bar{1}1}\,, \qquad S^q_{\bar{2}\bar{2}} = S^q_{22}\,, \qquad S^q_{\bar{1}3} = -S^q_{\bar{1}3}\,, \\ S^q_{\bar{2}3} &= -S^q_{\bar{2}3} \quad \left(S^q_{1\bar{1}}\,,\ S^q_{2\bar{2}} \text{ are independent}\right)\,. \end{aligned} \tag{7}$$

The 1 and $\bar{1}$ modes are decoupled from 2 and $\bar{2}$, since they correspond to different b.c. (see Stage (A), Subsection 5.1). Thus $S^q_{\bar{1}2}=0$, etc. What we really need is

* S^q_{33} *is for* TEM b.c., *while* $\widetilde{S}^q_{33}$ *is for* TE11 b.c.

the half-junction S-matrix, denoted S^h_{ij}. As is easy to see, the independent nonzero elements are related to S^q thus ($\bar{3}$ now denotes the rectangular mode at the $y_{\rm min}$ port):

$$\begin{aligned} S^h_{ij} &= S^q_{ij}\,, \quad i,j = 1,\bar{1} \text{ or } 2,\bar{2}\quad , \\ S^h_{3i} &= S^q_{3i}\,, \quad i = 1,2,\bar{1} \text{ or } \bar{2}\quad , \\ S^h_{\bar{3}i} &= S^q_{3i}\,, \quad i = 1 \text{ or } \bar{1}\quad , \\ S^h_{\bar{3}i} &= -S^q_{3i}\,, \quad i = 2 \text{ or } \bar{2}\quad , \\ S^h_{33} &= \frac{1}{2}\left(S^q_{33}+\widetilde{S}^q_{33}\right)\,, \quad S^h_{\bar{3}\bar{3}} = S^h_{33}\quad , \\ S^h_{3\bar{3}} &= \frac{1}{2}\left(S^q_{33}-\widetilde{S}^q_{33}\right)\,. \end{aligned} \tag{8}$$

We next re-introduce the shorts on the half-function. These are at $y_{\rm min}=-Y$ and $z_{\rm max}=Z$, with Y, Z given above in terms of $y_{\rm stub}$, $z_{\rm stub}$. We send an incoming TEM mode at the $z_{\rm min}$ port (that is, a '1' mode), and demand that the outgoing TE11 (or '2') mode have vanishing amplitude. This "zero asymmetry" condition becomes, once the short conditions are imposed:

$$S^h_{22}+S^h_{2\bar{2}} = -e^{2i\beta_2 Z}\quad , \tag{9}$$

where $\beta_2=\beta$ (TE11) , given above. Consulting our HFSS results for the S^q matrix (Table 1), we find that the L.H.S. of Eq. (9) is a complex number of unit modulus (a phase), which allows (9) to be satisfied. This is no coincidence; when both the 2 and $\bar{2}$ modes are excited with equal amplitudes, one must have $E_z=0$ at the rectangular port by $z\rightarrow -z$ symmetry, and hence $\left|S^h_{22}+S^h_{2\bar{2}}\right|=1$ with no outgoing power in WR90.

Equation (9) can be solved for Z: in inches,

$$2\,\beta_2\,(Z-0.3) \;=\; 0.2445 + 2\,\pi m \;\;, \tag{10}$$

with m an integer. Note that $z_{\rm stub}$ is thus independent of $y_{\rm stub}$, as advertised. Below we choose $m = 1$, which yields:

$$z_{\rm stub} = 0.7352 \text{ inch} \quad . \tag{11}$$

We repeat here the relation of (Y, Z) to $(y_{\rm stub}, z_{\rm stub})$:

$$\begin{aligned} -\,Y = y_{\rm min} \;&=\; -r_{\rm out} - y_{\rm stub} \quad , \\ Z = z_{\rm max} \;&=\; h/2 + z_{\rm stub} \quad , \end{aligned} \tag{12}$$

with $h = 0.4$ inches the WR90 height.

The theoretical expression for the TEM $\rightarrow$ TEM reflection amplitude, simplified via the zero-asymmetry condition, reads:

$$R \;=\; S^h_{11} - \frac{\left(S^h_{1\bar{1}}\right)^2}{S^h_{11} + \;\exp\;(2i\beta_1 Z)} - \frac{\left(S^h_{13}\right)^2 \rho^2}{2\,\sigma} \quad , \tag{13}$$

where

$$\begin{aligned} &\beta_1 \;=\; \beta\,(\text{TEM}) \;\;, \qquad \beta_3 \;=\; \beta\,(\text{TE10}) \quad , \\ &\rho \;=\; \left(S^h_{11} + S^h_{1\bar{1}} + \exp\,(2i\beta_1 Z)\right) \Big/ \left(S^h_{11} + \exp\,(2i\beta_1 Z)\right) \quad , \\ &\sigma \;=\; S^h_{33} + \exp\,(-2i\beta_3 Y) + \left(S^h_{23}\right)^2 \frac{1}{2S^h_{2\bar{2}}} - \frac{\left(S^h_{13}\right)^2}{2\left(S^h_{11} + \exp\,(2i\beta_1 Z)\right)} \quad . \end{aligned} \tag{14}$$

A Fortran program was written to evaluate R, and to optimize Y (per given Z), by minimizing $|R|$. [Notice that different 'm' values in (10) yield different R values, due to the $\exp(2i\beta_1 Z)$ phase appearing in (13),(14)]. The $||S^h||$ matrix used in this program is taken from Table 1, in conjunction with Eqs. (8). An (at least locally) optimal Y value is found at

$$y_{\rm stub} = 0.426 + 0.631\;n \text{ inches} \;\;, \tag{15}$$

where n is another integer (the $y_{\rm stub}$ increment is a half-wavelength of the WR90 mode). The value of $|R|$ at this stub length is predicted by the program to be 0.33, whereas the correct value is 0.77 (see Table 2, which lists the sidearm S-matrix at $z_{\rm stub} = 0.7352$ inches and $y_{\rm stub} = 0.426$ inches, as computed by HFSS, with estimated error of about 0.02). We attribute the discrepancy to evanescent modes near the junction and shorts. We note, however, that Table 2 also shows an asymmetric reflection coefficient of 0.04, in good agreement with the simple theory presented above. Also significant is the insensitivity of this latter coefficient to changes in $y_{\rm stub}$, as found from numerous HFSS and MAFIA simulations of the sidearm.

We next discuss the choice of ring dimensions and upstream location, which is again facilitated by theoretical considerations. For the S-matrix of the separate ring, the TEM and TE11 modes obviously decouple; only the TEM matrix is relevant, as the sidearm by itself chokes the dipole mode quite effectively.

The theory of the matching of ring and sidearm to produce a vanishing TEM $\rightarrow$ TEM reflectance for the full structure is a simple one: let r be the TEM reflection amplitude of the ring, and t the TEM transmission. The reference planes for either are chosen as the two z = const. planes bounding the ring. Let R again be the TEM reflectance of the sidearm (Table 2), but with a phase correction factor $\exp(2i\beta_1 \times 0.2$ inch), due to a

change of reference plane from that of Table 2 to the low-z plane of the WR90. Further, let L be the distance between ring and WR90. The condition of zero overall TEM reflection is easily found (e.g., via summation of an infinite geometric sum) to be:

$$e^{2i\beta_1 L} = R\left(r - \frac{t^2}{r}\right) \quad . \tag{16}$$

This can always be satisfied for some L, provided the R.H.S. is a pure phase. We found that for ring dimensions:

$$r_{\text{ring}} = 0.695 \text{ inches} \quad \text{(outer radius)} \ ,$$

$$\Delta z = 0.150 \text{ inches} \quad \text{(ring thickness)} \ , \tag{17}$$

$\text{Re}(tr^*) = 0, |r| \approx |R| = 0.77$. This guarantees that the R.H.S. of Eq. (16) is indeed approximately a pure phase; (16) then implies a value for L,

$$L = 1.5995 + 0.517\, k \text{ inches} \quad , \tag{18}$$

with k yet another integer. For $k = 0$, we have $L = 1.5995$.

The ring and junction are then sufficiently separated so the effects of evanescent modes are small; Indeed, the overall TEM reflection amplitude of the output structure is only ≈ 0.18 (see Table 3). Table 3 also shows results from HFSS for y_{stub}, z_{stub}, r_{ring}, Δz, and L as given by Eqs. (11), (15) (for $m = 1$, $n = 0$), (17), and (18). Results from a broadband (rise-time $= 90f^{-1}$, $f = 11.42$ GHz) MAFIA time-domain simulation for the same geometry are given by Figs. 4–5.

We thank Norman Kroll, Terry Lee, and Robert Palmer for numerous useful discussions, and the Accelerator Theory group at SLAC for their hospitality.

Table 1

Quarter-junction geometry S-matrix computed by HFSS. Reference planes are at ports. S-matrix elements are displayed as ordered pairs (modulus, phase).

S^q–Matrix Elements

TEM boundary condition

	3	1	$\bar{1}$
3	(.620, −143°)	(.555, 179°)	(.555, 179°)
1	(.555, 179°)	(.225, −177°)	(.801, −29°)
$\bar{1}$	(.555, 179°	(.801, −29°)	(.225, −177°)

TE11 boundary condition

	3	2	$\bar{2}$
3	(.431, −149°)	(.638, 13°)	(.638, −167°)
2	(.638, 13°)	(.307, −152°)	(.706, −172°)
$\bar{2}$	(.638, −167°)	(.706, −172°)	(.307, −152°)

Table 2

Sidearm S-matrix (High Frequency Structure Simulator run), displayed as ordered pairs (modulus, phase). The $z_{\min}$ reference plane is at the center of the WR90 (rectangular) waveguide. The TE10 mode propagates in the rectangular waveguide; the other two modes propagate in the coaxial waveguide.

S–Matrix Elements

	TE10	TE11	TEM
TE10	(.773, 94°)	(.016, −52°)	(.634, −147°)
TE11	(.016, −52°)	(.999, −175°)	(.043, −100°)
TEM	(.634, −147°)	(.043, −100°)	(.772, 153°)

Table 3

The S-matrix of the overall output structure (coax-ring-sidearm) depicted in Fig. 2, computed by High Frequency Structure Simulator. The modes are as in Table 2. S-matrix elements are displayed as ordered pairs (modulus, phase).

S–Matrix Elements

	TE10	TE11	TEM
TE10	(.177, 106°)	(.006, −158°)	(.984, 82°)
TE11	(.006, −158°)	(1.00, 101°)	(.005, 156°)
TEM	(.984, 82°)	(.005, 156°)	(.177, −123°)

Figure Captions

Fig. 1. HFSS plot of the Coax–Ring–Sidearm coupler (half structure).

Fig. 2. Same geometry as in Figure 1, with the dimensions of our optimal design.

Fig. 3. The Quarter–Junction Structure geometry.

Fig. 4. MAFIA time domain plot of reflection amplitude for coaxial TEM mode, for optimal design.

Fig. 5. As in Figure 4, but for the TEM to TE11 coaxial reflection amplitude; vertical scale is in units of 10^{-2}.

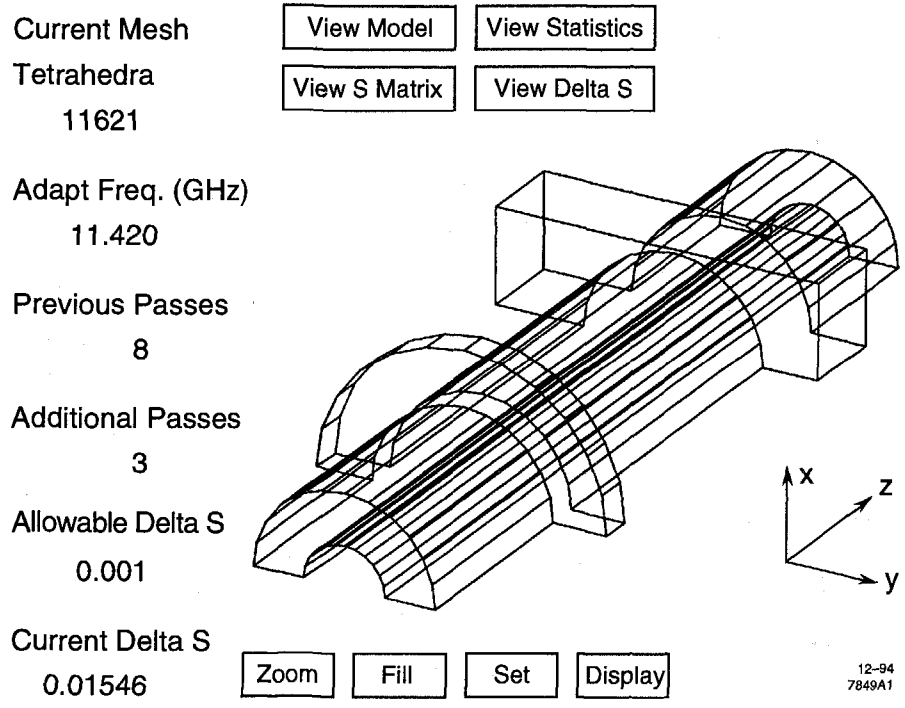

Fig. 1

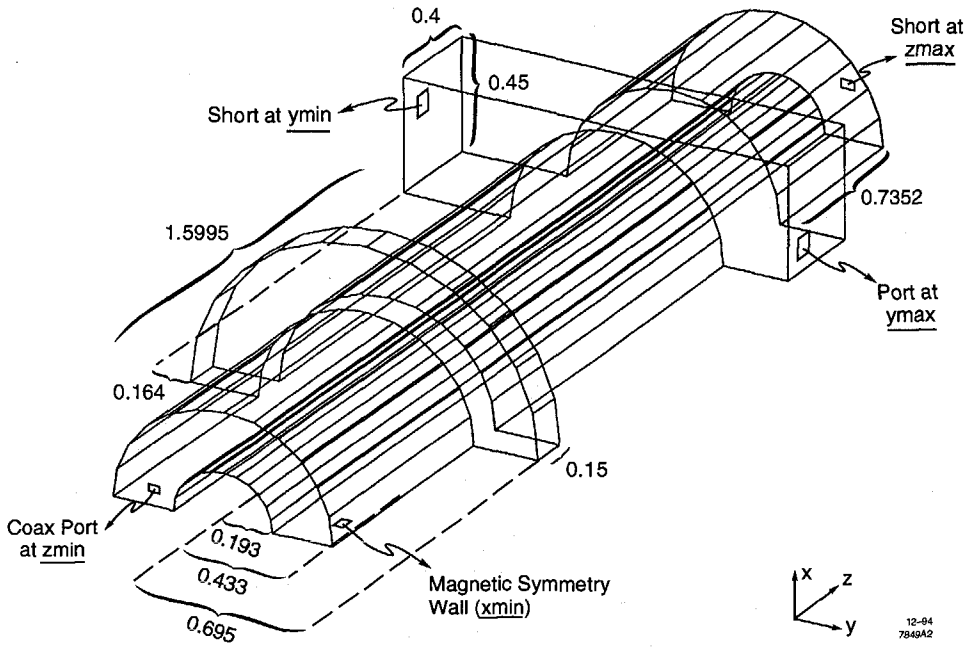
0.4
0.45
Short at ymin
Short at zmax
0.7352
1.5995
Port at ymax
0.164
0.15
Coax Port at zmin
0.193
0.433
0.695
Magnetic Symmetry Wall (xmin)
x
z
y
12-94
7849A2

Fig. 2

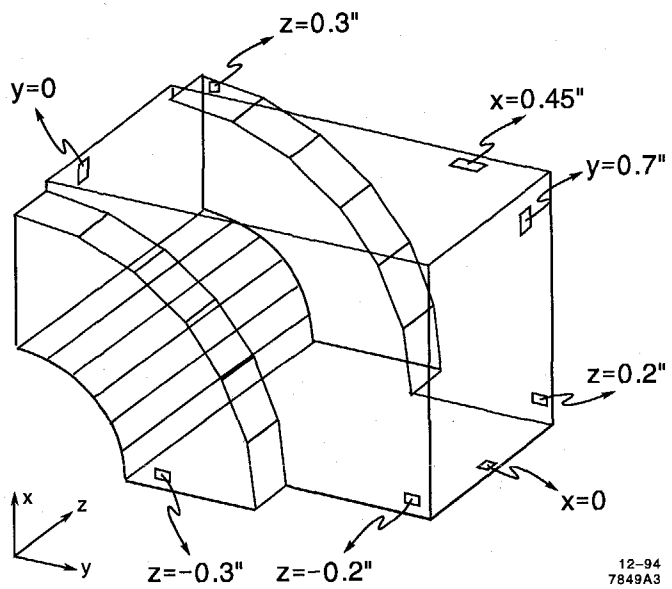
z=0.3"
y=0
x=0.45"
y=0.7"
z=0.2"
x=0
x
z
y
z=−0.3"
z=−0.2"
12-94
7849A3

Fig. 3

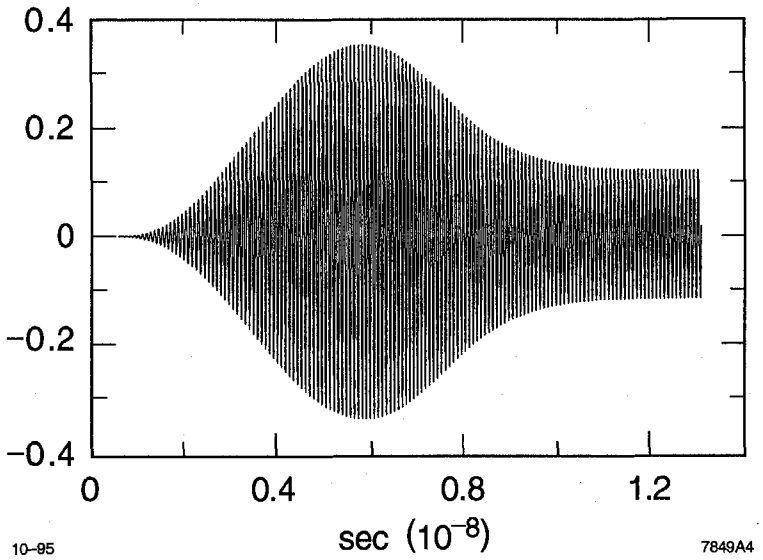
0.4
0.2
0
−0.2
−0.4
0
0.4
0.8
1.2
sec (10−8)
10–95
7849A4

Fig. 4

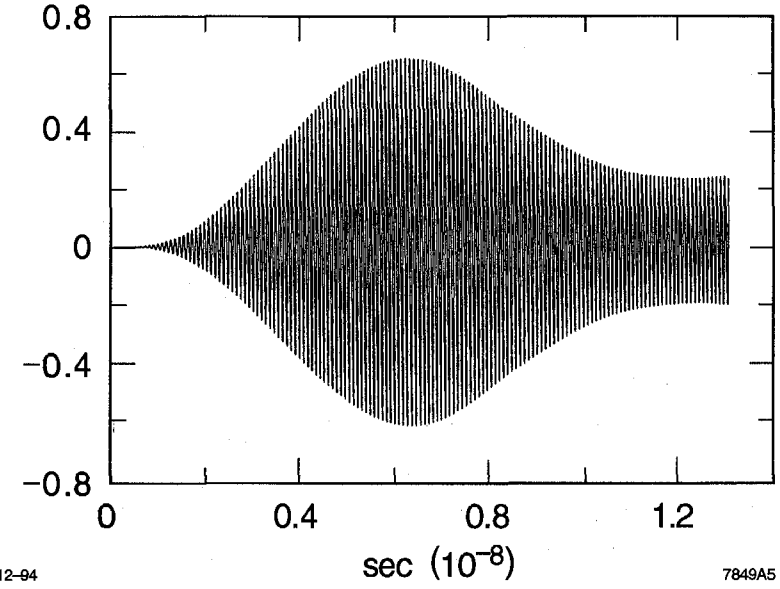
0.8
0.4
0
−0.4
−0.8
0
0.4
0.8
1.2
sec (10−8)
12–94
7849A5

Fig. 5